

3 The Phase Behaviour of 1-Alkyl-3-Methylimidazolium Ionic Liquids

KEIKO NISHIKAWA

Division of Nanoscience, Graduate School of Advanced Integration Science,
Chiba University, Japan

ABSTRACT

Some of the unique properties of room temperature ionic liquids are remarkably manifest in their thermal behaviour, viz. they exhibit low melting points despite being salts, difficulty in crystallisation, premelting over a wide temperature range, excessive supercooling, and complex thermal histories. In addition, 1-alkyl-3-methylimidazolium ionic liquids show peculiar thermal behaviour at the phase changes, namely “rhythmic melting and crystallisation,” “intermittent crystallization,” in the premelting regions, and ultra-slow phase changes. These thermal behaviours could be detected only by the use of an ultra-sensitive differential scanning calorimeter with nano-Watt stability, and simultaneous measurements of calorimetry and Raman scattering. This unique thermal behaviour is attributed to the flexibility of the alkyl chains bonded to the imidazolium ring, and linkage of the phase transition or structural relaxation with the conformational changes.

3.1 PHASE TRANSITIONS LINKED WITH CONFORMATIONAL CHANGES OF CATIONS

Ionic liquids are attracting much attention because of their characteristic properties [1–4] and potential utilities as functional liquids [5–10]. Their unique properties are particularly exhibited in their thermal behaviour, such as

premelting over a wide temperature range, excessive supercooling, various crystal–crystal phase transitions, and the existence of complex thermal histories [11–21]. Researchers have performed thermal analyses of ionic liquids and their crystals using differential scanning calorimetry (DSC), thermogravimetric analysis (TGA), and so on [11–21]. These studies have provided useful information regarding their thermal properties. In this chapter, we focus specifically on the thermal behaviour of 1-alkyl-3-methylimidazolium ionic liquids and their crystals, especially their phase behaviour.

Many experimental results have suggested that the existence of multiple conformers for a constituent ion seriously affects the structural and thermal properties of the ionic liquid. For ionic liquids, the importance of a variety in conformational structures of constituent ions was first recognised by Holbrey et al. [22] and by the Hamaguchi group [23, 24] independently. The two groups pointed out the existence of polymorphism in $[\text{C}_4\text{mim}]\text{Cl}$ crystals. In the former paper, Holbrey et al. concluded that the multiple conformers inhibit the easy crystallisation of ionic liquids [22]. Berg reviewed the existence of various conformers in liquids and their crystals for many ionic liquids [25]. Raman spectroscopic studies backed up by density functional theory (DFT) calculations revealed that the occurrence of multiple conformers of 1-alkyl-3-methylimidazolium ions and their populations are different in the liquid and crystalline states [1, 26–30]. With an apparatus for ultra-sensitive DSC [17, 31], and simultaneous measurements of DSC and Raman spectroscopy [29], my group also confirmed that the melting and crystallisation of $[\text{C}_4\text{mim}]\text{Br}$ and $[\text{C}_4\text{mim}]\text{Cl}$ occurred directly linked with the cooperative conformational change of the butyl group in the cation [17, 29]. Moreover, not limited to $[\text{C}_4\text{mim}]\text{Br}$ and $[\text{C}_4\text{mim}]\text{Cl}$, we affirm that most curious thermal behaviour of 1-alkyl-3-methylimidazolium ionic liquids is due to the link between the phase transitions and the conformational changes of the alkyl chains bonded to the imidazolium ring [17, 18, 20, 21, 29, 32, 33].

Some examples on the varieties of conformers of 1-alkyl-3-methylimidazolium cations, and the relationships between conformational changes and phase behaviour, are presented in the following sections. Prior to their detailed discussion, the conformers of the three cations, $[\text{C}_2\text{mim}]^+$, $[\text{C}_3\text{mim}]^+$ {1-(2-propyl)-3-methylimidazolium cation}, and $[\text{C}_4\text{mim}]^+$, are outlined briefly here.

3.1.1 Conformers of 1-Alkyl-3-Methylimidazolium Cations

Stable and possible conformational structures for the three cations $[\text{C}_2\text{mim}]^+$, $[\text{C}_3\text{mim}]^+$, and $[\text{C}_4\text{mim}]^+$ in gaseous state can be obtained by DFT calculation using the Gaussian03 program package [34]. The quantum mechanical calculations suggest that there exist several rotational isomers for each of these cations: $[\text{C}_2\text{mim}]^+$ [27], $[\text{C}_3\text{mim}]^+$ [30], and $[\text{C}_4\text{mim}]^+$ [35, 36]. Taking into account both energy differences among isomers, and results from single crystal structure analyses of the corresponding salts, however, we can pick up a limited number of rotational isomers as possible conformers for each cation in their

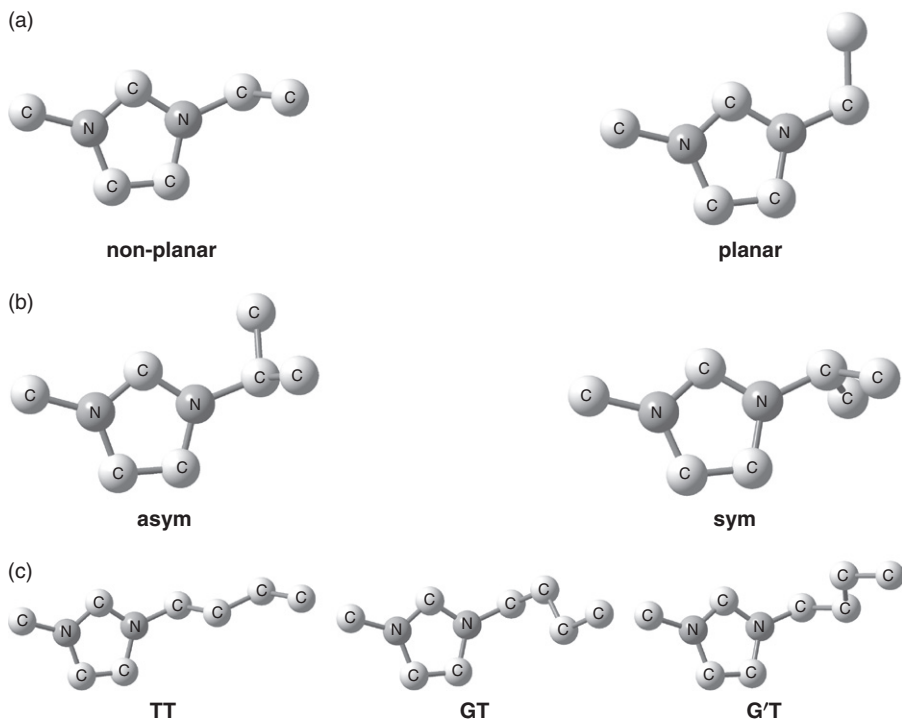


Figure 3.1 Stable conformers for (a) $[\text{C}_2\text{mim}]^+$, (b) $[\text{C}_3\text{mim}]^+$, and (c) $[\text{C}_4\text{mim}]^+$.

crystal or liquids states. The conformers to be borne in mind are shown in Figure 3.1. For $[\text{C}_2\text{mim}]^+$, Figure 3.1a, two rotational isomers around the N1-C1' axis are stable, namely **planar** and **non-planar** conformers [27]. The change of potential energy accompanying the rotation around the N1-C1' axis is shown in Figure 3.2a. It is seen that the **non-planar** conformer is about 2 kJ mol^{-1} more stable than the **planar** conformer in the free cation. In fact, the **non-planar** conformation is adopted in most crystals of 1-alkyl-3-methylimidazolium salts, including for the simple $[\text{C}_2\text{mim}]^+$ cation. It is characteristic that the energy barrier from non-planar to planar is very small.

For the $[\text{C}_3\text{mim}]^+$ ion [30], there exist two possible conformers: the symmetric form (**sym**) and the asymmetric form (**asym**). As shown in Figure 3.1b, **sym** refers to the arrangement where two methyl groups in the isopropyl group are positioned symmetrically with respect to the imidazolium ring. For the **asym** conformer, the plane formed by N1-C1'-C2' is almost perpendicular to the plane of the imidazolium ring. Figure 3.2b shows the potential energy for the rotation of the isopropyl group of $[\text{C}_3\text{mim}]^+$ around the N1-C1' axis, as calculated by DFT. The dihedral angle of C5-N1-C1'-H is defined as the torsion angle. The two local minima, at torsion angles of *ca.* 30° and 180° , correspond to **asym** and **sym**, respectively.

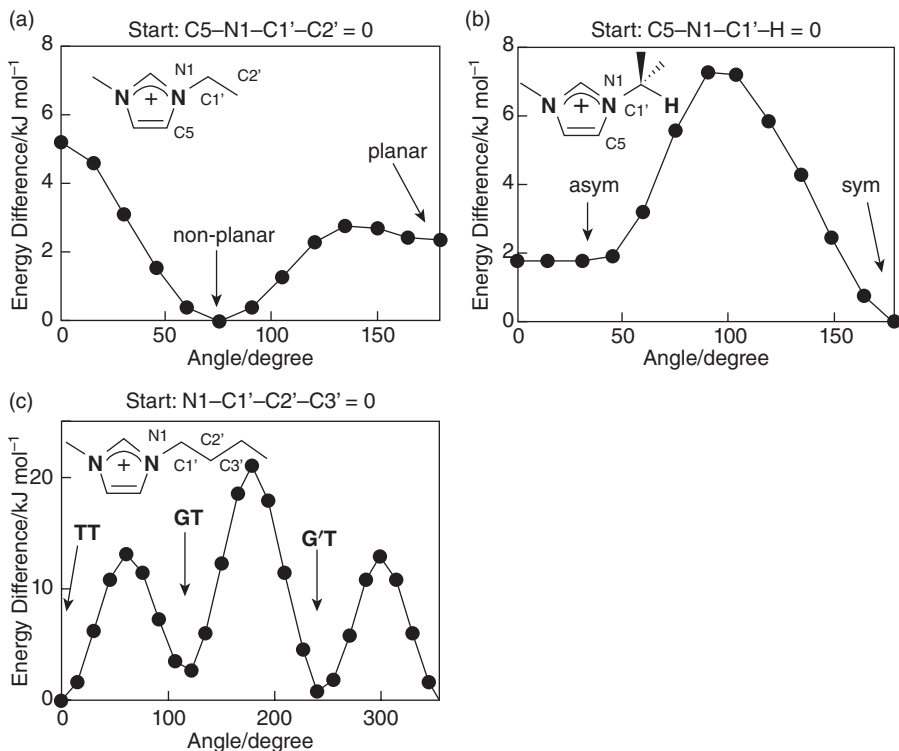


Figure 3.2 Potential energies as functions of torsion angles: (a) $[\text{C}_2\text{mim}]^+$, (b) $[\text{C}_3\text{mim}]^+$, and (c) $[\text{C}_4\text{mim}]^+$.

There are three rotational isomers as possible conformers for $[\text{C}_4\text{mim}]^+$ in the crystal or liquid states among nine or more conformers [35, 36], that is, the *gauche trans* (**GT**), *trans trans* (**TT**), and *gauche' trans* (**G'T**) conformations. They are caused by the rotation of the butyl group around the $\text{C}1'-\text{C}2'$ axis, keeping the arrangement for the $\text{C}2'-\text{C}3'$ axis in the *trans* conformation. These three isomers are shown in Figure 3.1c. Figure 3.2c shows the potential energy change accompanied with rotation around the $\text{C}1'-\text{C}2'$ axis.

3.1.2 DSC Measurements of the Bromides of $[\text{C}_2\text{mim}]^+$, $[\text{C}_3\text{mim}]^+$, and $[\text{C}_4\text{mim}]^+$

The DSC traces for $[\text{C}_2\text{mim}]\text{Br}$ [37], $[\text{C}_3\text{mim}]\text{Br}$ [18], and $[\text{C}_4\text{mim}]\text{Br}$ [17] are shown in Figure 3.3a,b,c, respectively. The bromides were selected as the standard samples to focus solely on the conformations of 1-alkyl-3-methylimidazolium cations. To avoid contamination, such as from unreacted precursor materials, the salts were recrystallised, and single crystals were selected for starting samples. The crystals were dried sufficiently under a vacuum of about 10^{-2} Pa.

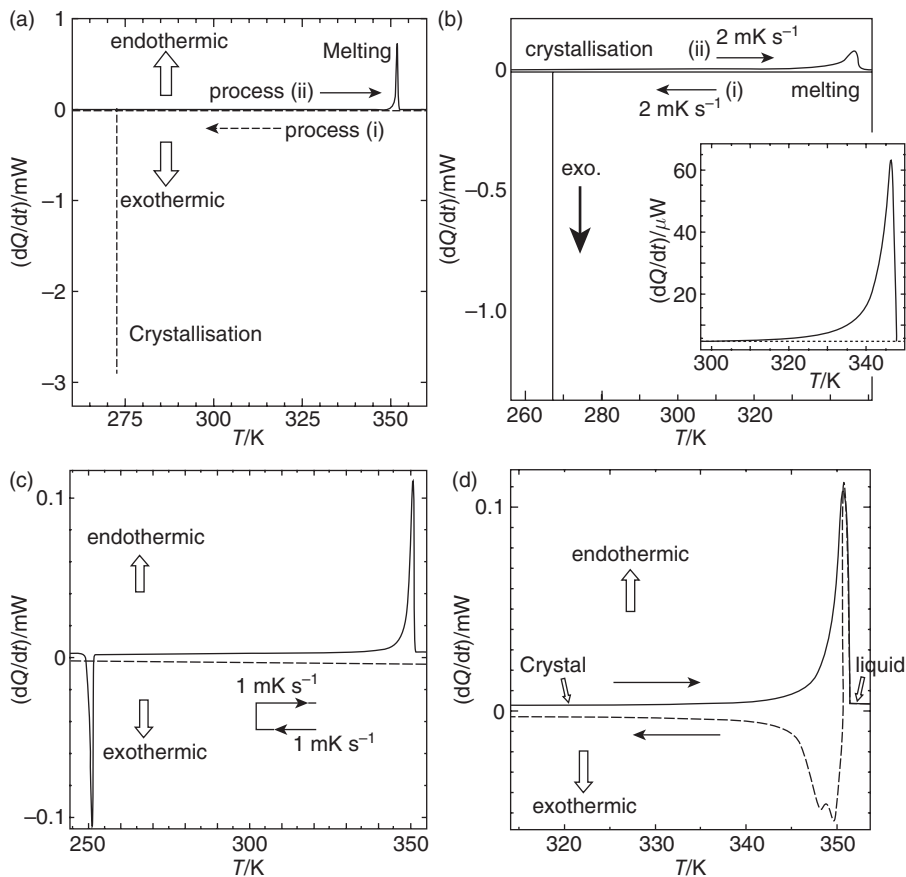


Figure 3.3 Overall DSC traces of (a) [C₂mim]Br, (b) [C₃mim]Br, and (c) [C₄mim]Br. (d) DSC curves for [C₄mim]Br around the melting point. The broken curve shows the trace where the sample is cooled on the way to the premelting process. The heating and cooling rate are 1 mK s⁻¹.

The DSC traces of [C₂mim]Br are shown in Figure 3.3a [37]. The sample was cooled from 360 K (liquid state) to 223 K, and then heated from 223 to 360 K at the scanning rate of 2 mK s⁻¹. The salt crystallised at 273 K in the cooling process (broken line) and melted at 352 K in the heating process (solid curve). Raman spectroscopic measurements revealed that [C₂mim]⁺ in the crystalline state of the bromide is in the non-planar form, while both planar and non-planar conformers are mixed in the liquid and supercooled liquid states [27].

Figure 3.3b indicates the DSC traces of [C₃mim]Br obtained at the cooling and heating rates of 2 mK s⁻¹ [18]. The exothermic crystallisation peak appeared at about 267 K in the cooling process, Process (i), and the endothermic melting

peak appeared at about 346 K in the heating process, Process (ii). As found for $[\text{C}_2\text{mim}]\text{Br}$, $[\text{C}_3\text{mim}]\text{Br}$ crystallises in the cooling process and melts in the heating process. From this viewpoint, these two salts are more “normal” than $[\text{C}_4\text{mim}]\text{Br}$ (discussed later). The crystallisation of $[\text{C}_3\text{mim}]\text{Br}$ occurs at about 80 K lower than melting, indicating the stable existence of a supercooled state and that it is hard to crystallise. The same characteristic feature has been reported for many ionic liquids [11–17, 20, 21]. As shown in Figure 3.3b, the melting peak has a very broad range, extending beyond 20 K, while the crystallisation peak is sharp. The magnified drawing around the melting peak is illustrated in the inset in Figure 3.3b. Contamination of a sample commonly causes broadening of its DSC melting curve. To avoid the effect of contamination, several different single crystals were selected for study—the sample was pure enough to crystallise as single crystals. However, the peak is too broad to regard this melting as a simple process of loosening of the crystalline lattices. We conclude that this broadening is due to premelting, characteristic of these samples, as well as other ionic liquids. In comparison with a similar broad temperature range observed during the premelting of $[\text{C}_4\text{mim}]\text{Br}$ [17], we assumed that the structural changes of the $[\text{C}_3\text{mim}]^+$ cations occurred during both the melting and crystallisation processes. Our Raman spectroscopic experiments [30] confirmed that the conformation of the $[\text{C}_3\text{mim}]^+$ ions in the crystalline state is **asym**, while **sym** and **asym** coexist in the liquid and supercooled liquid states and that a conformational change between the two occur in the premelting region, as expected.

The DSC traces for $[\text{C}_4\text{mim}]\text{Br}$ are shown in Figure 3.3c [17]. In the measurement, crystalline $[\text{C}_4\text{mim}]\text{Br}$ was first melted completely by heating, cooled down to 223 K as shown by broken line, and then heated up to 360 K as shown by a solid curve. The cooling and heating rates were 1 mK s^{-1} . No peak was found in the cooling process. However, in the heating process exothermic and endothermic peaks were found at about 250 and 350 K, respectively. That is, during the cooling process from the liquid, the liquid or supercooled liquid state continued down to the lowest temperature of the experiment (223 K) and crystallisation did not occur. In the heating process, crystallisation was observed at about 250 K and the crystal melted at about 350 K.

It is noted that the melting peak is broad, ranging over several Kelvin. This peak is too broad to regard this melting as a simple process. We thus suggest that this broadness is due to premelting, characteristic of the present sample. $[\text{C}_4\text{mim}]\text{Br}$ appears as only one crystal form, in which the $\text{C}1'-\text{C}2'-\text{C}3'$ conformation of the butyl group is in **GT** [22], while both of the **GT** and **TT** conformations coexist in liquid and supercooled liquid states [26, 29]. As a result, some of the cations must change their conformation from **GT** to **TT** upon melting, and vice versa at the crystallisation. We consider that this premelting behaviour is due to the increase of some fluctuation in the libration around the C-C bonds (especially $\text{C}1'-\text{C}2'$) within the potential minimum. This triggers the cooperative changes of conformation in the butyl chain and leads to

melting. Our Raman spectroscopic experiments confirmed that a part of the $[\text{C}_4\text{mim}]^+$ ions with **GT** conformation change in the premelting region [29].

From the magnified DSC curve around the crystallisation point (not shown here), it was noted that the crystallisation peak is divided into two. In Figure 3.3c, the specimen in the temperature region below the crystallisation peak is in a supercooled liquid phase, in which both of the **GT** and **TT** conformers coexist [26, 29]. On the other hand, $[\text{C}_4\text{mim}]\text{Br}$ in the temperature region above that of this peak is in the crystalline phase, where only the **GT** conformer exists [22, 26, 29]. Taking into consideration the structural change of the cation mentioned above, we interpret the observed split in the crystallisation peak as being due to the dynamics of crystallisation, namely the $[\text{C}_4\text{mim}]^+$ ions with the **GT** conformation and Br^- anions crystallise initially, while the $[\text{C}_4\text{mim}]^+$ ions with the **TT** conformation do not form crystals until after they have changed conformation from **TT** to **GT**. The lower-temperature component of the peak can be assigned to the direct crystallisation of **GT** conformers, and the component at the higher temperature to the crystallisation of **TT** conformers after the change of conformation from **TT** to **GT**. Of course, these changes of the conformation must be cooperative to form a crystal. A large number of cations must cooperatively change their conformations. As a result, the dynamics of crystallisation of $[\text{C}_4\text{mim}]^+$ ions with the **TT** configuration is slow enough to be detected separately. As the experiment was performed at a constant heating rate of 1 mK s^{-1} , the temperature difference of the two separate components corresponds to the time required for the cooperative change of conformers from **TT** to **GT**; it was about 5 minutes. We anticipated that the same change in the conformation occurs in the melting process. Indeed, when we reversed the heating process to cooling in the premelting region, we observed the split in the peak. Figure 3.3d shows the trace of the experiments, where the sample was first heated to a point in the premelting region (solid line), and then was cooled (broken line). The heating and cooling rates for the traces were 1 mK s^{-1} . As is evident in the figure, the splitting of the peak was also observed. This splitting was more remarkable for the sample which was heated up nearly to the top of the melting curve. The peak of higher temperature is assigned to the direct crystallisation of the portion which locally melts with **GT** conformers and that of lower temperature corresponds to the crystallisation of the portion with **TT** conformers after the change of conformation to **GT**.

3.2 SUITABLE EQUIPMENT FOR THE THERMAL ANALYSIS OF IONIC LIQUIDS

Many types of equipment for thermal analyses are commercially available and give useful information regarding the thermal properties of samples. If the sample is an ionic liquid, however, the closest attention must be paid to the

sensitivity/stability of the equipment, and to the capability of setting experimental conditions. This is because the thermal behaviour of ionic liquids is generally very complex, and thermal histories are frequently exhibited in their responses. Some phenomena occur at an unbelievably slow speed, which is thought to be related to the complex thermal histories of the ionic liquids. Without recognising the extremely slow changes, some thermal measurements of ionic liquids were performed at scanning speeds, which were much more rapid than their relaxation rates. This is thought to be one of the origins of confusion in thermal data reported for ionic liquids. Here, two laboratory-constructed scanning instruments are introduced, which are suitable for the thermal analyses of ionic liquids.

The first example is a nano-Watt-stabilised DSC instrument of the heat-flux type, which was designed and constructed by Tozaki [17,31]. The design is based on the following concepts: thermoelectric modules are utilised for a heat-flux sensor (the Seebeck effect) and heat pumps (the Peltier effect), and the system adopted for temperature regulation is a type of predictive controller [38] instead of a proportional integral derivative (PID) controller. In this system, the amount of the current passed into the Peltier elements to supply or remove heat is predicted both from the difference between the actual sample temperature and the set temperature, and from the temperature history up to the starting point of regulation. We have programmed this procedure to repeat every 2 seconds. This controller causes no ripples because no on-off switching is used. By setting up multiple adiabatic boxes around a sample, this DSC instrument can measure a heat flow with a baseline fluctuation within ± 3 nW. This baseline stability, which corresponds to the sensitivity of the DSC, is 10^2 – 10^3 times higher than that of commercially available DSC equipment [31]. This apparatus is also designed to scan as slowly as ~ 0.01 mKs $^{-1}$, enabling us to mimic a nearly quasi-static process. This scanning speed corresponds to taking 28 hours to raise the temperature by 1 K. As the relaxation time of the apparatus is estimated to be ~ 2 seconds, the dynamics of a thermal process can be traced for a relaxation time exceeding 2 seconds. Measurements can be made during either process, heating or cooling, by changing the direction of the electric current through the thermoelectric modules. This performance is essential for thermal measurements on ionic liquids, since many of them often display different behaviour during the cooling and heating processes. The measurable temperature region of the DSC instrument is from 220 to 453 K, and the rate of cooling or heating is controllable in the range from 0.01 to 10 mK s $^{-1}$. The temperature of the sample was measured using a platinum resistance thermometer. The heat flow measurement was performed with a 1% margin. The temperature was controlled within ± 0.15 mK.

The second example is the equipment for simultaneous measurements of DSC and Raman spectroscopy [29]. The outline of the apparatus is as follows. The laboratory-made calorimeter is combined with the commercially available Raman spectrometer. The spectrometer is a fibre optically coupled Raman spectrometer (Hololab, Kaiser Optical Systems) equipped with a GaAlAs

diode laser (wavelength: 785 nm). The optical resolution is 4 cm⁻¹, and a spectrum in the range of 100 to 3450 cm⁻¹ can be measured simultaneously due to the adoption of a multiplex grating system backed up by a charge coupled device (CCD) camera. As for the calorimeter, thermoelectric modules are used both as a heat flux sensor and as a heat pump. A free piston stirring cooler is applied to obtain low temperatures, down to 153 K. Temperature is measured using a platinum resistance thermometer. The baseline stability of the calorimetry trace is measured as being 5 μW. One of the characteristics of the calorimeter is its capability of carrying out heating and/or cooling experiments at an extremely slow rate, sufficient for mimicking a quasi-static condition. From the standpoint of Raman spectroscopy, this apparatus can be regarded as a sample holder by which spectra at various temperatures ranging from 153 to 403 K can be obtained under sufficiently stabilised thermal conditions. From the standpoint of calorimetry, the apparatus gives us direct information on the structure change of the sample during accompanying thermal phenomena. Laser power was set at less than 10 mW for simultaneous measurements to observe the *in situ* thermal behaviour of ionic liquids.

3.3 THE PHASE BEHAVIOUR OF [C₄mim][PF₆]

The phase behaviour of [C₄mim][PF₆] is introduced here as an example of where complicated crystal–crystal transitions occur accompanied with various conformational changes of the butyl group in the [C₄mim]⁺ cation [20]. [C₄mim][PF₆] is one of the most popular ionic liquids because it consists of representative cations and anions. There are hence reports on the liquid [39–41] and crystalline [42, 43] structures for [C₄mim][PF₆]. For the crystal structure, two groups independently obtained crystals belonging to the same crystalline phase, and reported that the butyl group of the cation is in the **G'T** conformation, as shown in Figure 3.1c [42, 43]. From thermodynamic studies, some groups indicated that [C₄mim][PF₆] has two crystal polymorphs [42, 44–48] and complex phase transition behaviour [42, 46, 48]. However, there was some confusion about the phase behaviour in previous reports.

We investigated the phase transition behaviour and cation structures of [C₄mim][PF₆] by calorimetry and Raman spectroscopy equipped with a precise temperature-control stage [20]. Consequently, we found that [C₄mim][PF₆] has three crystal polymorphs, and all the phase transitions except the glass transition occur accompanied by conformational changes of the butyl group around the C1'-C2' axis.

3.3.1 Phase Transitions

Measurements were carried out using the apparatus described in Section 3.2, which made it possible to perform simultaneous measurements of calorimetry and Raman spectroscopy [29].

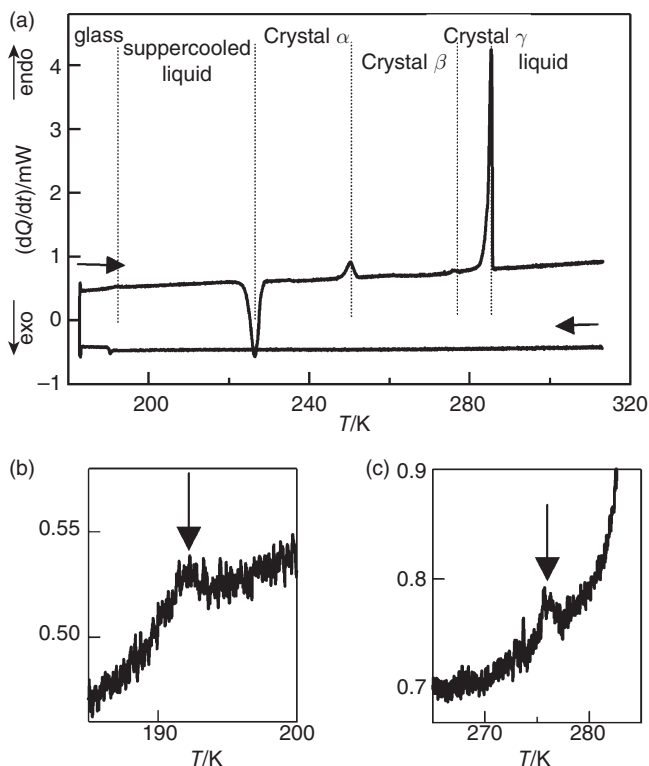


Figure 3.4 (a) Calorimetric curve for $[C_4mim][PF_6]$ at a scanning rate of 5 mK s^{-1} for the whole temperature range. Expanded curves: (b) around the glass transition and (c) around the phase transition from **Crystal β** to **Crystal γ** .

Figure 3.4 shows calorimetric curves for $[C_4mim][PF_6]$ in the range of 183–313 K. To follow and match the relatively slow thermodynamic changes of ionic liquids, the measurements were performed at a scan rate of 5 mK s^{-1} , which was much lower than the rates in typical calorimetric measurements. In the cooling process, no phase transition peak appeared except for the glass transition. On the other hand, several phase transition peaks were observed (Fig. 3.4) in the heating process, such as the glass transition (192 K), crystallisation (226.5 K), two crystal–crystal transitions (250.3 K, 276 K), and melting (285.3 K). The temperature values in parentheses are peak-top values. The temperature for the glass transition during heating is in good agreement with that obtained by adiabatic calorimetry, at 190.6 K [44]. We called the three observed crystalline phases **Crystal α** , **Crystal β** , and **Crystal γ** in order of increasing temperature.

We focus now on the crystal–crystal phase transitions. As mentioned earlier, there are two endothermic peaks at 250.3 and 276 K in the calorimetric curve

between the crystallisation and melting peaks. Most other groups detected only the signal corresponding to our larger peak at 250.3 K, and they reported that [C₄mim][PF₆] had two crystalline phases [42, 47]. We think that the peak at 276 K is difficult to detect by DSC measurements with typical scanning rates because it is a very small peak that appears close to the melting peak, and the phase change seems to occur very slowly. Although the signal at 276 K is very small, we can clearly distinguish two phases under our experimental conditions, and the two phases have different structures, as shown in the next section.

3.3.2 Cation Structure in Each Phase

The structure of the [C₄mim]⁺ ion in each crystalline phase was studied by Raman spectroscopy [20]. The results are shown in Figure 3.5a. Raman bands in the range of 580–640 cm⁻¹ are known as marker bands for rotational isomers of the butyl group in the [C₄mim]⁺ ion [23, 26]. The existence of nine rotational isomers of [C₄mim]⁺ was demonstrated by quantum chemical calculations [35, 36]. Taking into account both energy differences among the isomers and results from single crystal structure analyses for [C₄mim]⁺ salts [20, 24, 42, 43, 49, 50], we can pick three rotational isomers as possible conformers for [C₄mim]⁺ in the crystal or liquid states, that is, **GT**, **TT**, and **G'T** conformations caused by the rotation of the butyl group around the C1'-C2' axis. The three isomers are shown in Figure 3.1c, and the corresponding active Raman bands from DFT calculations are displayed in Figure 3.5b,c,d.

Crystal β has a distinguishable band at 624 cm⁻¹, which can be assigned to the **TT** conformation of [C₄mim]⁺, Figure 3.5c [23, 26]. In the region of 580–640 cm⁻¹, the Raman spectrum of **Crystal α** is similar to that of **Crystal γ**. They have characteristic peaks at about 500, 600, and 700 cm⁻¹, suggesting that the cation structures in these crystalline phases will be assigned to **GT**, Figure 3.5b [23], or **G'T**, Figure 5d, conformations. The difference between **Crystal α** and **Crystal γ** is found in the region of 300–350 cm⁻¹. From the DFT calculations for [C₄mim]⁺, the Raman bands observed at higher frequency (338 cm⁻¹) and lower frequency (326 cm⁻¹) are attributed to the **GT** and **G'T** conformations, respectively. As a result, **Crystal α** can be assigned to **GT**, and **Crystal γ** to **G'T**.

It should be noted that a small component due to the **G'T** conformation exists in **Crystal α**. We studied the temperature dependence of the Raman scattering intensities of **Crystal α**. The upper spectrum in Figure 3.5a was measured at 229 K after crystallisation during heating. The second spectrum was obtained from **Crystal α** at 193 K during cooling. As expected, no phase transition occurred in the cooling process. If **GT** and **G'T** conformers coexist in an asymmetric unit in **Crystal α**, the intensity ratio of the bands at higher (338 cm⁻¹) and lower (326 cm⁻¹) frequencies will not change. However, the band intensity at 326 cm⁻¹ originating from **G'T** clearly decreases with falling temperature. This indicates that the most stable conformer in **Crystal α** is **GT**, and we conclude that the conformation of the cation in **Crystal α** is **GT**. We

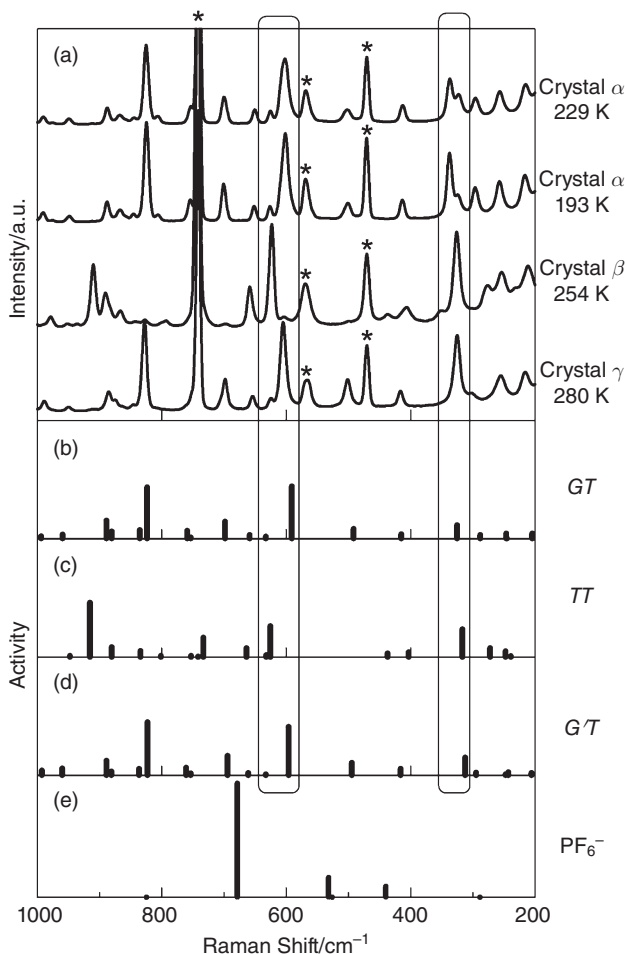


Figure 3.5 (a) Observed Raman spectra for the three crystalline phases (asterisks indicate the anion bands). (b)–(d) Raman active bands, calculated with DFT, for the **GT**, **TT**, and **G'T** conformations of $[\text{C}_4\text{mim}]^+$, respectively. (e) Raman active bands, calculated with DFT, for $[\text{PF}_6]^-$.

consider two possibilities for the origin of the appearance of **G'T**: (1) the rotational isomerism reaction between **GT** and **G'T** easily occurs in **Crystal α** (i.e., there is a low activation energy for rotational isomerism), or (2) part of the **G'T** conformer was left as amorphous solid or liquid without crystallisation. We often observe the coexistence of crystals and supercooled liquid in ionic liquids. Although not reported yet, we have recently found from a combination measurements of nuclear magnetic resonance (NMR) and Raman spectroscopy that **Crystal α** changes to **Crystal γ** even at *ca.* 227 K (crystallisation temperature from the supercooled liquid) when **Crystal α** is kept for a

long time (such as one day). This observation supports possibility (1) for the origin. This phenomenon shows that the phase transitions of ionic liquids are in general extremely slow and that our observation of their thermal behaviour is strongly dependent on the thermal histories of the samples.

The [C₄mim]⁺ ion in the [C₄mim][PF₆] crystalline phase was reported to take the **G'T** conformation from single crystal structure analyses at 173 K [43] and 193 K [42]. These results seem to be inconsistent with our finding because the **G'T** conformer appears in **Crystal** γ , which is the highest-temperature crystalline phase. However, this apparent inconsistency can be resolved by the complex thermal history of [C₄mim][PF₆] [46]. Moreover, we measured Raman spectra of **Crystal** γ at 193 K (not shown), which were obtained by cooling from **Crystal** γ with no phase transition. Two research groups grew single crystals by different methods [42, 43]. We suppose that the crystals they first made were **Crystal** γ and that their structures were retained as the temperatures were lowered to the measurement temperatures without a phase transition.

Figure 3.6 shows the temperature dependence of Raman spectra during melting. This region includes the phase transition from **Crystal** γ (**G'T**) to liquid. The band at 624 cm⁻¹ that is assigned to the **TT** conformation arises through melting, and behaviour such as the appearance or disappearance of bands characteristic to each conformation were observed in other phase transition regions. Therefore, we can conclude that all phase transitions of [C₄mim][PF₆], except for the glass transition, accompany conformational change of the butyl group. It is noted that structural change in the cation becomes abruptly active just near the peak-top temperature of melting, although the premelting

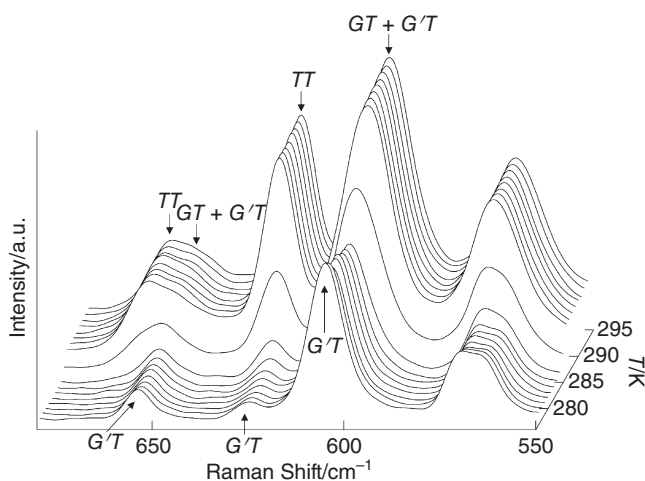


Figure 3.6 Temperature dependence of Raman spectra near the melting point of [C₄mim][PF₆]. The scanning rate was 5 mK s⁻¹, and each spectrum was obtained every 1 K.

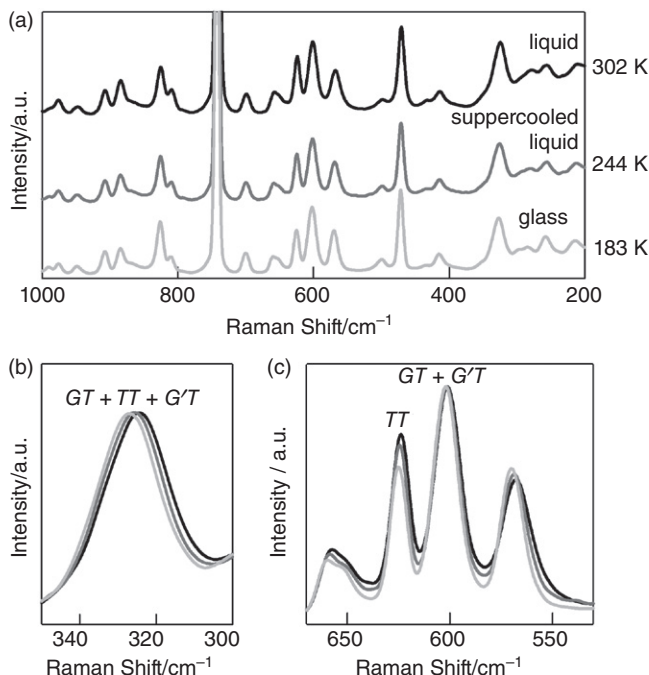


Figure 3.7 Raman spectra of $[\text{C}_4\text{mim}][\text{PF}_6]$ in liquid (302 K), supercooled liquid (244 K), and glass states (183 K) in the ranges of (a) 200–1000 cm^{-1} , (b) 300–350 cm^{-1} , and (c) 530–670 cm^{-1} .

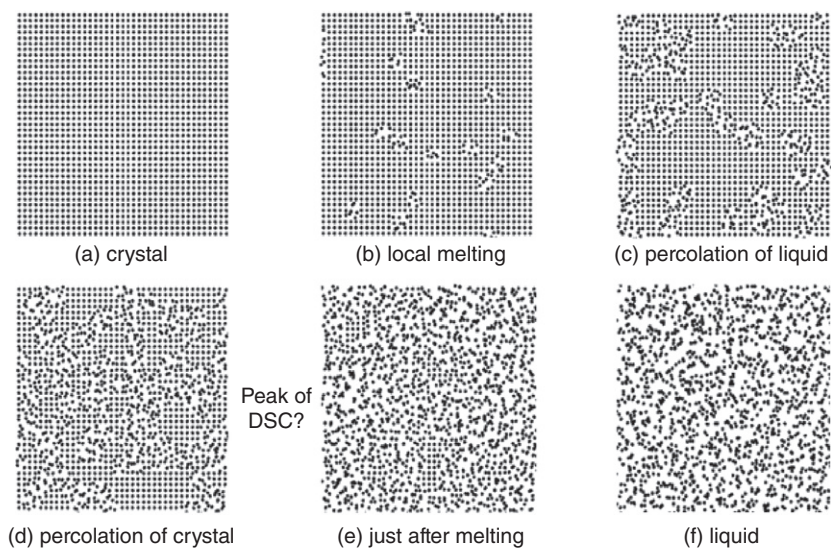
phenomenon starts at a temperature 4–5 K lower. The same tendencies were observed in the melting processes of $[\text{C}_4\text{mim}]\text{Br}$ [29] and $[\text{iC}_3\text{mim}]\text{Br}$ [30]. In our reported results on ionic liquids [18, 29, 30], the conformational changes of constituent ions seem to be delayed after the start of the thermal signal of the phase transitions.

Figure 3.7a shows the Raman spectra of $[\text{C}_4\text{mim}][\text{PF}_6]$ in the liquid (at 302 K), supercooled liquid (at 244 K in the cooling process), and glass (at 183 K) states [20]. These spectra resemble each other, and this demonstrates that the three states are composed of cations with similar structure. According to the Raman spectra in the ranges of 300–350 cm^{-1} , (Fig. 3.7b) and 530–670 cm^{-1} (Fig. 3.7c), the **GT**, **TT**, and **G'T** conformers are considered to be mixed in these states, as in other 1-alkyl-3-methylimidazolium ionic liquids.

Many crystal structures have been reported for a range of $[\text{C}_4\text{mim}]^+$ salts [22, 24, 42, 43, 49–51]. Some typical data are summarised in Table 3.1. The cation conformations in these crystal structures are concentrated in the **GT** conformation. Our Raman scattering study shows the existence of three types of crystalline phase for $[\text{C}_4\text{mim}][\text{PF}_6]$, where conformations of the cation differ. No report has been made of 1-butyl-3-methylimidazolium ionic liquids with

TABLE 3.1 Cation Conformations in Crystal Structures of $[C_4mim]X$ Obtained by X-ray Diffraction.

| | | | | | | | |
|--------------|---------------|-----------|-----------|-----------------|-----------------|-----------------|----------------|
| Anion | $Cl^{22,24}$ | Br^{22} | I^{50} | Tf_2N^{49} | $CH_3SO_3^{51}$ | $CH_3SO_4^{51}$ | $PF_6^{42,43}$ |
| Conformation | TT, GT | GT | GT | GT + G'T | GT | GT | G'T |

**Figure 3.8** A schematic model for melting and crystallisation.

all three conformations, **GT**, **TT**, and **G'T**, in their measured crystal structures. $[C_4mim][PF_6]$ is one of the most representative examples showing the conformational variety of ionic liquids. At the same time, the complex isomerisation of the constituent cations has caused some confusion regarding the phase behaviour and thermodynamic properties of $[C_4mim][PF_6]$.

3.4 NOVEL PHASE TRANSITION BEHAVIOURS OF ROOM TEMPERATURE IONIC LIQUIDS

3.4.1 A Model for Melting and Crystallisation

Following our results on $[C_4min]Br$ [17, 29] and $[^iC_3mim]Br$ [18, 30], we have modelled the melting and crystallisation behaviour of ionic liquids, and the schematic diagram of the model is shown in Figure 3.8. In a crystalline state, ions with a certain specific conformation are arranged regularly (Fig. 3.8a). In the heating process, small domains in a crystalline area start to melt first,

accompanied by conformational changes of the ions, probably at the regions with crystalline defects or at the surface/boundary of the crystals (Fig. 3.8b); specifically, local melting occurs and the regions are composed of mixtures of different conformers. These premelting domains grow as the temperature is increases (Fig. 3.8c) until percolation of the crystal areas finally breaks off (Fig. 3.1d). Up to such a temperature, local melting and crystallisation in the pre-melting region can occur reversibly by heating or cooling [17, 18]. We may assume that many small crystalline domains remain even after the melting (Fig. 3.8e), where the DSC trace falls to the baseline level of the liquid. The reverse phenomena will be observed in the crystallisation process from the liquid.

The above-mentioned processes are considered to occur not only in ionic liquids, but also in “normal” substances. However, the phenomena in ionic liquids can be detected with the supersensitive DSC equipment because their phase transitions are extremely slow.

3.4.2 Rhythmic Melting and Crystallisation

We performed detailed measurements, focussing on the melting process of $[C_4mim]Br$ [32]. As shown in Figure 3.3c, the salt has a wide premelting region. The single crystal melted perfectly, cooled down to room temperature, and in turn heated at the rate of 0.02 mK s^{-1} from room temperature to 355 K. This heating rate corresponds to 13.9 hours to raise the temperature of the sample by 1 K.

The melting trace of $[C_4mim]Br$ is shown in Figure 3.9a, where the data collected every 40 seconds are plotted as dots. As shown in the figure, the DSC curve is very noisy. Selecting five representative regions in the curve, we numbered the divisions around 344.5, 345.9, 349.6, 351.2, and 353.2 K as (1), (2), (3), (4), and (5), respectively. Divisions (1) and (2) correspond to the regions near and just on the starting point of premelting, respectively. Division (3) corresponds to the middle point of the premelting curve, and the trace is noisiest in this region. Division (4) is the point where the crystal just melts. Division (5) corresponds to the region where the sample is stabilised as the liquid state. Figure 3.9b and Figure 3.9c are expanded representations of Divisions (3) and (5). Each dot in the expanded plots refers to the measuring point, which is carried out every 4 seconds. Therefore, the lateral axes correspond to time axes as well as temperature axes.

We have made frequency analyses for 5000 points in each Division, by drawing the baseline and measuring the deviation of each peak-top from the base line. As for Divisions (1) and (5), the distribution curves by the frequency analysis are regarded almost perfectly as Gaussian functions. And the half widths at $1/e$ of the peak-tops are about 3–4 nW. Thus, the deviations of Divisions (1) and (5) represent statistical thermal/electronic noise of the apparatus, and just refer to the sensitivity or resolution of the DSC equipment [31]. On the other hand, other curves slightly differ from the Gaussian distributions,

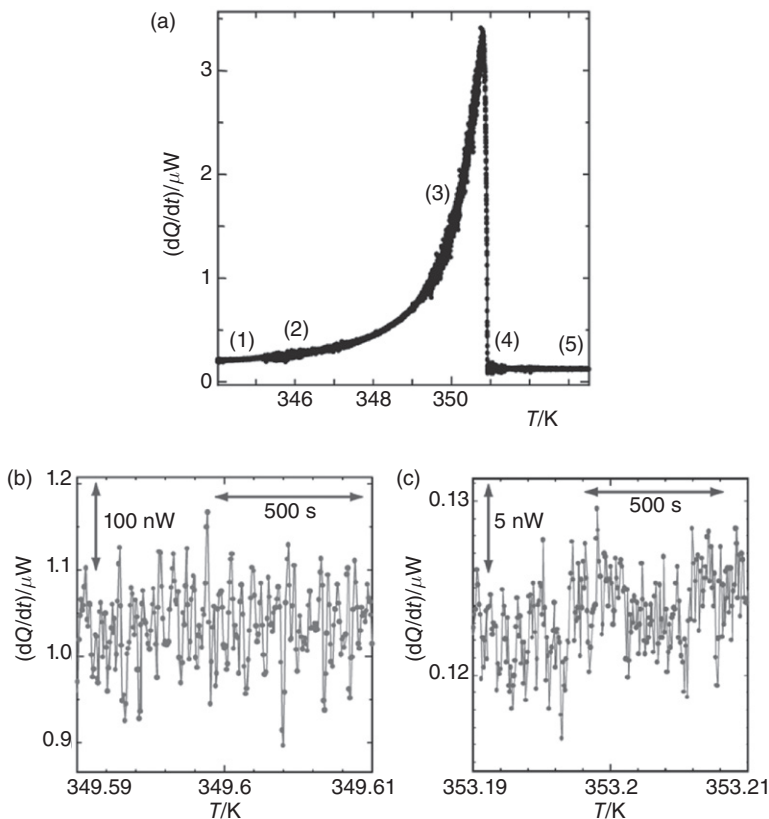


Figure 3.9 (a) DSC trace of $[\text{C}_4\text{mim}]\text{Br}$ near the melting point. The heating rate is 0.02 mK s^{-1} . Five divisions are selected and numbered as (1)–(5). (b) Expanded figure of the division (3). (c) Expanded figure of the division (5). Dots in (b) and (c) refer to the measuring points of every 4 seconds.

and the widths are wider than the width due to intrinsic noises. Therefore, we can conclude that the states of Divisions (2), (3), and (4) are not in thermodynamic equilibrium, and the deviation is not noise, and has some physical meanings.

To understand the present results, the two following facts should be borne in mind. First, the premelting with over 10 K accompanies the conformational change of the butyl group from **GT** to **TT**, as well as the changes in the crystal-line lattice [17, 29]. Second, *ab initio* calculations showed that the energy difference between **GT** and **TT** conformations is within $\pm 1 \text{ kJ mol}^{-1}$ [35, 36]. Such a small energy difference implies that the conformational change for a free ion occurs easily. Therefore, the Divisions (2) and (3) will denote that, by the local temperature increase due to the fluctuation of the heating, a part of the

$[\text{C}_4\text{mim}]^+$ ions change their conformation from **GT** to **TT** in a domain and the domain melts, corresponding to Figure 8b. As only a small thermal energy is supplied because of the extremely slow heating rate, the thermal energy is absorbed by the melting domain itself, and the neighbouring one, which is just going to melt. The crystallisation of the domain then occurs. In turn, thermal energy is released by the crystallisation. Using this energy and the supplied energy from the thermoelectric modules, a part of the crystalline domain melts. These processes can be repeated rhythmically. The rhythmic melting and crystallisation appear as “noise” on the DSC trace, as shown in Figure 3.9a,b. Just after melting, namely in Division (4) in Figure 3.9a, the aggregation domains where most of the ions are in the **GT** conformation are going to crystallise again, or a great number of ions are going to change their conformations between **TT** and **GT**. In other words, the “noisy” trace of Division (4) indicates that the state is non-equilibrium. Ions in the domains are going to rhythmically crystallise or melt even at higher temperature than the melting one. We should note that the DSC pattern (frequency or heat flow magnitude) of the change at just the melting point, Division (4), is almost the same as the pattern at the starting point of the premelting shown in Division (2).

The number of ion pairs of $[\text{C}_4\text{mim}]\text{Br}$ in the domains can be estimated from the frequency distribution curves. The total enthalpy of the melting is reported to be 23.0–23.6 kJ mol⁻¹ [17]. If we assume that each peak or valley in the expanded figures refers to the melting or crystallising of a domain, and regard the half-width of the distribution curve at 1/e as the averaged value of the heat flow, the number of ion pairs of $[\text{C}_4\text{mim}]^+$ and Br^- in a domain is 2.0×10^{12} for Divisions (2) and (4), and 1.8×10^{13} for Division (3). This number of ion pairs corresponds to a radius of 4.9×10^3 nm for Divisions (2) and (4), and 1.0×10^4 nm for Division (3), if the domains are assumed to be spheres. This study was the first to estimate the domain size relating to the melting or crystallisation of ionic liquids [32].

From the expanded curves, the timescale of melting/crystallisation of the domain can be obtained, because the interval of measured points in the expanded figures corresponds to 4 seconds and 0.08 mK. For Divisions (1) and (5), the widths of the oscillatory peaks are randomly distributed in the range of 4–60 seconds. On the other hand, the widths of the corresponding peaks of Divisions (2), (3), and (4) are similar to each other; the half-width values of the equivalent peaks in (2), (3), and (4) are 12–16 seconds, 12–20 seconds, and 8–12 seconds, respectively. These values correspond to the timescales of the rhythmic transition of the domains. It is reported that several minutes are necessary to achieve equilibrium for the portions of the two conformers of **GT** and **TT** in $[\text{C}_4\text{mim}]\text{Cl}$ by the instant melting [1]. The long relaxation time of the present phase transition could be due to the accompanying cooperative conformational change of a large number of ions, of the order of 10^{12} – 10^{13} . As shown here, a supersensitive thermodynamic measurement is a very effective method to detect such slow dynamic behaviour involving heat flow. The present heating rate matches well to the slow dynamics.

This curious phenomenon was named “rhythmic melting and crystallisation” [32], which was observed in the premelting region in the heating process of $[\text{C}_4\text{mim}]\text{Br}$. Melting and crystallisation are periodically repeated with the endothermic and exothermic heat transfer cycles that alternately trigger subsequent changes. A rhythmic change of volume phase transition in polymer gels is well known [52]. Because the structures of the ions are relatively simple compared with polymers, the observed phase transition in an ionic liquid is unique. We think that the main origin of the rhythmic melting and crystallisation of the ionic liquid is a coupling of the melting/crystallisation and cooperative conformational change of the ions.

3.4.3 Intermittent Crystallisation

The next sample to be considered is $[\text{C}_3\text{mim}]\text{Br}$ [18, 33], the overall DSC traces of which are shown in Figure 3.3b. To investigate the details of the premelting phenomenon of the sample, we performed cyclic experiments. Namely, the sample was heated at the rate of 2 mK s^{-1} from room temperature to the preset temperature, Process (1), and then cooled down, Process (2). The temperature, set at a specific point in the premelting region, is hereafter denoted as the “returning temperature.” We performed numerous experiments varying the returning temperature and the cooling rate, and some novel phenomena were observed depending on the experimental conditions. Two of them are introduced here.

When the returning temperature was the peak-top temperature of the melting DSC trace and the cooling rate was set at 0.05 mK s^{-1} , a very curious phenomenon was observed. The result is shown in Figure 3.10a, where the

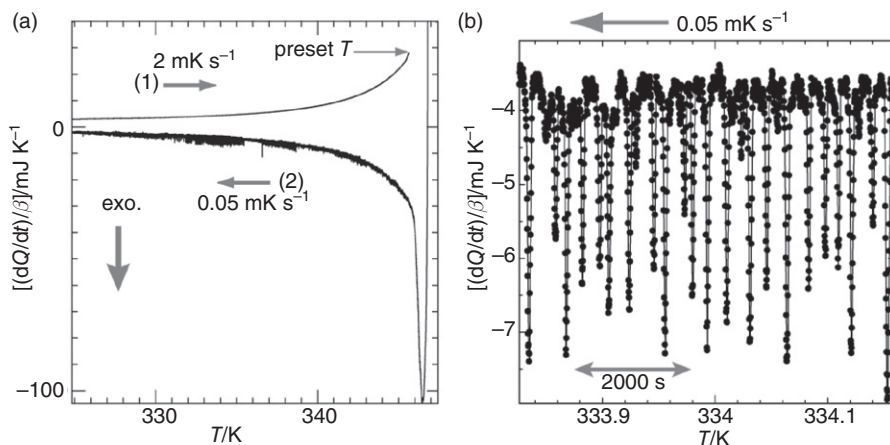


Figure 3.10 The DSC traces for $[\text{C}_3\text{mim}]\text{Br}$ around the melting point. The curve shows the trace wherein the sample was cooled down from 346.0 K. (a) Full-scale results, and (b) a magnified section of data around 334 K in the cooling run.

values of the vertical axis are divided by the heating or cooling rate (β) to normalise the rate differences. The DSC signals of the reversible crystallisation traced simple curves with accompanying fine exothermic spikes. The magnified drawing around 334 K is shown in Figure 3.10b. The small peaks were sharp, and were separated piece by piece. Moreover, all of them were exothermic peaks. In the latter figure, the data are plotted as dots every 4 seconds. As emphasised in our papers [18, 32, 33], these notched peaks are not due to electronic noise, but intrinsically arise from the present sample. We have named this phenomenon “intermittent crystallisation” [33]. The present DSC instrument, with super-high sensitivity and quick response times, has enabled us to detect this phenomenon. These results reveal that there exist local melting domains in the premelting region, as indicated in the schematic model, shown in Figure 3.8b, and that the domains with almost the same order in size are spatially separated from each other at about 334 K. The spikes refer to the crystallisation of the domains.

For $[\text{C}_3\text{mim}]\text{Br}$, more than 90% of the crystalline area seemed to melt up to the returning temperature, as estimated from the amount of absorbed heat. Being cooled down suddenly, most of the $[\text{C}_3\text{mim}]^+$ and Br^- ions appear to be smoothly crystallised, because the DSC trace is smooth just after returning, as shown in Figure 3.10a. The exothermic spikes appear after 70–80% release of the total enthalpy of crystallisation. This behaviour implies that a large number of $[\text{C}_3\text{mim}]^+$ ions in the premelting region maintained an **asym** conformation (i.e., the conformation in the crystalline phase) that leads to smooth crystallisation. This speculation is supported by our experimental studies involving simultaneous measurements of Raman spectroscopy and calorimetry [29]. The results for $[\text{C}_3\text{mim}]\text{Br}$ [30] and $[\text{C}_4\text{min}]\text{Br}$ [29] showed that a major portion of the conformational changes occurred at the temperature at the peak-top of the melting DSC trace, or just after this point. In the cooling process of $[\text{C}_3\text{mim}]\text{Br}$, these domains seemed to remain where **sym** and **asym** conformers are mixed together, suggesting that **sym** isomers cannot easily turn to an **asym** conformation.

We estimated the order of enthalpy for a domain in the intermittent crystallisation to be 0.7×10^{-5} J. Comparing with the molar crystallisation enthalpy of 13.9 kJ mol^{-1} , the average number of ion pairs in the domains was then estimated to be $\sim 3 \times 10^{14}$. The timescale of crystallisation can be estimated from Figure 3.10b. The interval of intermittent crystallisation was about 200–230 s, and about 100 s is required for each domain to crystallise under the present experimental conditions. These values are much longer than the relaxation time of the apparatus.

Once the returning temperature exceeded the peak-top temperature of the DSC trace, the observed phenomena altered drastically. First, we confirmed that the sample cooled from the temperature exceeding the peak-top did not entirely crystallise in the premelting region but overall crystallisation occurred at about 267 K, as shown in Figure 3.3b. This demonstrates that the upper

limit for the reversible melting and crystallisation is nearly at the peak-top temperature.

We discovered another unique phenomenon in the measurement performed at the returning temperature of 346.5 K and with a cooling rate of 0.05 mK s^{-1} . This temperature was just 0.2 K higher than the peak-top temperature. As shown in Figure 3.3b, at this temperature the melting curve did not drop to the baseline of the liquid state, meaning that the sample did not become liquid completely. The overall DSC traces of this experiment are shown in Figure 3.11a. As shown in this figure, a small exothermic peak first appeared in the cooling process. This seems to be assigned to the crystallisation of a very small portion. Crystalline grains remain at this temperature, and **asym** conformers, in a quantity enough to form crystals, remain [30]. However, the crystalline grains cannot grow up to become an overall crystalline state. We consider that this is because the percolation of the crystalline area breaks off—see the schematic model shown in Figure 3.8d. It is speculated that the flat region of the baseline in the cooling process refers to the coexisting state of supercooled liquid and crystalline grains. Although this may be thought to be a strange phenomenon, we often observe the stable coexistence of supercooled liquid and crystals for many ionic liquids.

Although overall crystallisation did not occur in the premelting region, the DSC trace was very noisy in some temperature ranges, as shown in Figure 3.11a. The magnified drawing around 340.52 K is shown in Figure 3.11b, where data for every 4 seconds are plotted as dots. The noise intrinsic to the apparatus was $\pm 3 \text{ nW}$. The observed spikes were about 10 times larger than the 6-nW

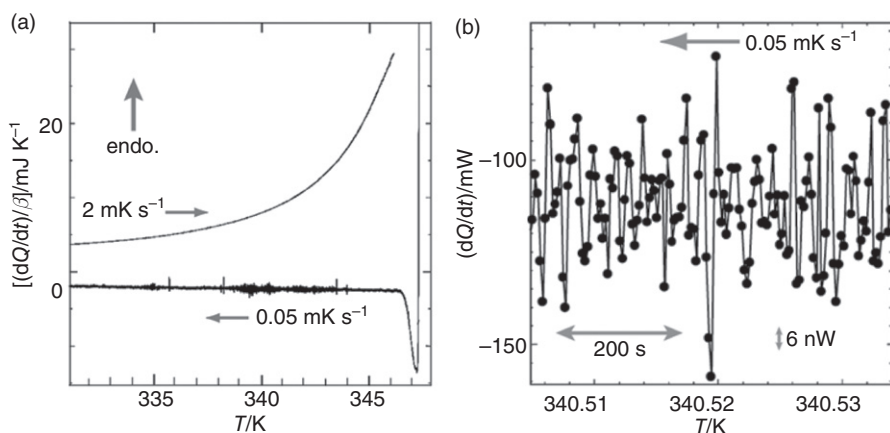


Figure 3.11 The DSC traces for $[\text{C}_3\text{mim}]\text{Br}$ around the melting point. The sample was cooled down with a cooling rate of 0.05 mK s^{-1} from a temperature of 0.2 K higher than the peak-top of the melting trace. **(a)** Full-scale data set, and **(b)** magnified section around 340.52 K.

margin shown by the arrow, and indicated that they were attributed to a thermal phenomenon characteristic of the sample. It is clear that the pattern of periodic endothermic and exothermic heat transfers is different from the pattern of intermittent exothermic heat transfers. The notched peaks are rhythmic crystallisation and melting, and we observed the same phenomenon for [C₄mim]Br in the premelting region and in the liquid region just after melting during the heating process, as described in Section 3.4.2. At the temperature slightly exceeding the peak-top for the case of [ⁱC₃mim]Br, it is thought that crystalline domains remain surrounded by a large amount of liquid areas and that the percolation of the crystalline area breaks off. However, it is supposed that thermal fluctuations easily occur around the remaining crystalline domains. The melted region around these remaining crystalline grains crystallises as cooling occurs. The heat released during crystallisation melts the neighbouring domains. Due to the endothermic process of melting, crystallisation occurs in turn. Crystallisation and melting are thereby repeated rhythmically. These were observed as the periodic spikes in the DSC trace, as shown in Figure 3.11a,b.

In the domains where the rhythmic crystallisation and melting occurred, $5-9 \times 10^{12}$ ion pairs were contained. The timescale of the phenomenon was estimated to be 10–20 seconds. Compared with the intermittent crystallisation where the returning temperature was preset at peak-top temperature (Fig. 3.10b), the released or absorbed heat in the rhythmic crystallisation and melting was smaller, and the timescale was correspondingly shorter. These results may be contrary to the expectation that the premelting domains should become larger in the returning experiment from 346.5 K, as seen in Figure 3.11a. However, as for the sample heated up to the temperature exceeding the peak-top, a large number of [ⁱC₃mim]⁺ ions changed to a **sym** conformation [30], and they mixed with the **asym** ions. As a result, it seems to be more difficult for larger domains to crystallise during the extremely slow cooling process. On the other hand, even a small amount of the heat released during local crystallisation will easily melt the small crystallising domains because of the large mixture of **sym** and **asym** conformations. This seems to be the reason for rhythmic crystallisation and melting occurring in the smaller size regions and with a shorter periodicity. By repeating rhythmic crystallisation and melting, the whole sample seems to relax into the supercooled liquid state.

3.5 CONCLUDING REMARKS

The thermal behaviour of some 1-alkyl-3-methylimidazolium ionic liquid is presented, with a focus on their phase transitions. In addition to the common thermal phenomena for most ionic liquids, such as premelting over a wide temperature range and excessive supercooling, the following unique thermal phenomena were observed:

1. Existence of thermal histories affecting their thermal behaviours.
2. Frequent existence of complex crystal–crystal phase transitions and/or polymorphism.
3. Extremely slow phase transitions.
4. Curious phenomena in phase transitions such as “rhythmic melting and crystallisation” and “intermittent crystallisation.”

These phenomena are generally observed for most ionic liquids, so the following discussion can be applied to most ionic liquids. Although the above-mentioned phenomena (1–4) are different, the origins of these behaviours must be closely related; that is, the conformational changes in the dense field are likely to affect the phase transitions and cause these phenomena. Multiple conformers for a constituent ion commonly exist in ionic liquids. Energies of some of the conformers are almost the same, and the small energy differences among them are strongly influenced by the types of counter ion and by interactions resulting from the relative positions and orientations of ions. In the liquid state, coexistence of multiple conformers is entropically profitable. Therefore, most phase transitions of ionic liquids link with the conformational changes of constituent ions. This link causes complex and curious phase transitions. Due to the Coulomb interactions, the density of an ionic liquid is generally 10–20% higher than that of a molecular substance with similar components. The decrease in the free volume for conformational changes is probably the major origin of the retarded phase transition for ionic liquids.

REFERENCES

- 1 Hamaguchi, H., and Ozawa, R., Structure of ionic liquids and ionic liquid compounds: Are ionic liquids genuine liquids in the conventional sense?, *Adv. Chem. Phys.* **131**, 85–104 (2005).
- 2 Wishart, J.F., and Castner, E.W. Jr. (eds.), *Physical Chemistry of Ionic Liquids*, Special Issue of *J. Phys. Chem. B* **111** (18), 4639–5029 (2007).
- 3 Rogers, R.D., and Voth, G.A. (eds.), *Ionic Liquids*, Special Issue of *Acc. Chem. Res.* **40** (11), 1077–1236 (2007).
- 4 Castner, E.W. Jr., and Wishart, J.F., Spotlight on ionic liquids *J. Chem. Phys.* **132**, Article ID 120901 (2010).
- 5 Welton, T., Room-temperature ionic liquids. Solvents for synthesis and catalysis, *Chem. Rev.* **99**, 2071–2083 (1999).
- 6 Rogers, R.D., and Seddon, K.R. (eds.), *Ionic Liquids—Industrial Applications for Green Chemistry*, ACS Symposium Ser., Vol. 818, American Chemical Society, Washington DC (2002).
- 7 Wasserscheid, P., and Welton, T. (eds.), *Ionic Liquids in Synthesis*, VCH-Wiley, Weinheim (2003).
- 8 Ohno, H. (ed.), *Electrochemical Aspects of Ionic Liquids*, John Wiley & Sons, Hoboken (2005).

- 9 Plechkova, N.V., and Seddon, K.R., Applications of ionic liquids in the chemical industry, *Chem. Soc. Rev.* **37**, 123–150 (2008).
- 10 Greaves, T.L., and Drummond, C.J., Protonic ionic liquids: Properties and applications, *Chem. Rev.* **108**, 206–237 (2008).
- 11 Holbrey, J.D., and Seddon, K.R., The phase behaviour of 1-alkyl-3-methylimidazolium tetrafluoroborates; ionic liquids and ionic liquid crystals, *J. Chem. Soc., Dalton Trans.* **13**, 2133–2139 (1999).
- 12 Ngo, H.L., LeCompte, K., Hargens, L., and McEwen, A.B., Thermal properties of imidazolium ionic liquids, *Thermochim. Acta* **357–358**, 97–102 (2000).
- 13 Huddleston, J.G., Visser, A.E., Reichert, W.M., Willauer, H.D., Broker, G.A., and Rogers, R.D., Characterization and comparison of hydrophilic and hydrophobic room temperature ionic liquids incorporating the imidazolium cation, *Green Chem.* **3**, 156–164 (2001).
- 14 Marsh, K.N., Boxall, J.A., and Lichtenthaler, R., Room temperature ionic liquids and their mixtures—a review, *Fluid Phase Equilib.* **219**, 93–98 (2004).
- 15 Nishida, T., Tashiro, Y., and Yamamoto, M., Physical and electrochemical properties of 1-alkyl-3-methylimidazolium tetrafluoroborate for electrolyte, *J. Fluorine Chem.* **120**, 135–141 (2003).
- 16 Fredlake, C.P., Crosthwaite, J.M., Hert, D.G., Aki, S.N.V.K., and Brennecke, J.F., Thermophysical properties of imidazolium-based ionic liquids, *J. Chem. Eng. Data* **49**, 954–964 (2004).
- 17 Nishikawa, K., Wang, S., Katayanagi, H., Hayashi, S., Hamaguchi, H., Koga, Y., and Tozaki, K., *J. Phys. Chem. B* **111**, 4894–4900 (2007).
- 18 Nishikawa, K., Wang, S., Endo, T., and Tozaki, K., *Bull. Chem. Soc. Jpn.* **82**, 806–812 (2009).
- 19 Triolo, A., Russina, O., Fazio, B., Appetecchi, G.B., Carewska, M., and Passerini, S., Nanoscale organization in piperidinium-based room temperature ionic liquids, *J. Chem. Phys.* **130**, Article ID 164521 (2009).
- 20 Endo, T., Kato, T., Tozaki, K., and Nishikawa, K., Phase behaviours of room temperature ionic liquid linked with cation conformational changes: 1-Butyl-3-methylimidazolium hexafluorophosphate, *J. Phys. Chem. B* **114**, 407–411 (2010).
- 21 Endo, T., Kato, T., and Nishikawa, K., Effects of methylation at the 2 position of the cation ring on phase behaviours and conformational structures of imidazolium-based ionic liquids, *J. Phys. Chem. B* **114**, 9201–9208 (2010).
- 22 Holbrey, J.D., Reichert, W.M., Nieuwenhuyzen, M., Johnston, S., Seddon, K.R., and Rogers, R.D., Crystal polymorphism in 1-butyl-3-methylimidazolium halides: Supporting ionic liquid formation by inhibition of crystallization, *Chem. Commun.* 1636–1637 (2003).
- 23 Hayashi, S., Ozawa, R., and Hamaguchi, H., Raman spectra, crystal polymorphism, and structure of a prototype ionic-liquid [bmim]Cl, *Chem. Lett.* **32**, 498–499 (2003).
- 24 Saha, S., Hayashi, S., Kobayashi, A., and Hamaguchi, H., Crystal structure of 1-butyl-3-methylimidazolium chloride. A clue to the elucidation of the ionic liquid structure, *Chem. Lett.* **32**, 740–741 (2003).

- 25 Berg, R.W., Raman spectroscopy and *ab-initio* model calculations on ionic liquids, *Mon. Chem.* **138**, 1045–1075 (2007), and references cited therein.
- 26 Ozawa, R., Hayashi, S., Saha, S., Kobayashi, A., and Hamaguchi, H., Rotational Isomerism and structure of the 1-butyl-3-methylimidazolium cation in the ionic liquid state, *Chem. Lett.* **32**, 948–949 (2003).
- 27 Umebayashi, Y., Fujimori, T., Sukizaki, T., Asada, M., Fujii, K., Kanzaki, R., and Ishiguro, S., Evidence of conformational equilibrium of 1-ethyl-3-methylimidazolium in its ionic liquid salts: Raman spectroscopic study and quantum chemical calculations, *J. Phys. Chem. A* **109**, 8976–8982 (2005).
- 28 Berg, R.W., Deetlefs, M., Seddon, K.R., Shim, I., and Thompson, J.M., Raman and *ab initio* studies of simple and binary 1-alkyl-3-methylimidazolium ionic liquids, *J. Phys. Chem. B* **109**, 19018–19025 (2005).
- 29 Endo, T., Tozaki, K., Masaki, T., and Nishikawa, K., Development of apparatus for simultaneous measurements of Raman spectroscopy and high-sensitivity calorimetry, *Jpn. J. Appl. Phys.* **47**, 1775–1779 (2008).
- 30 Endo, T., and Nishikawa, K., Isomer populations in liquids for 1-isopropyl-3-methyl-imidazolium bromide and its iodide, and their conformational changes accompanying the crystallizing and melting processes, *J. Phys. Chem. A* **112**, 7543–7550 (2008).
- 31 Wang, S., Tozaki, K., Hayashi, H., and Inaba, H., Nano-watt stabilized DSC and ITS applications, *J. Therm. Anal. Cal.* **79**, 605–613 (2005).
- 32 Nishikawa, K., Wang, S., and Tozaki, K., Rhythmic melting and crystallizing of ionic liquid 1-butyl-3-methylimidazolium bromide, *Chem. Phys. Lett.* **458**, 88–91 (2008).
- 33 Nishikawa, K., and Tozaki, K., Intermittent crystallization of an ionic liquid: 1-Isopropyl-3-methylimidazolium bromide, *Chem. Phys. Lett.* **463**, 369–372 (2008).
- 34 Frisch, M.J., Trucks, G.W., Schlegel, H.B., Scuseria, G.E., Robb, M.A., Cheeseman, J.R., Montgomery, J.A. Jr., Vreven, T., Kudin, K.N., Burant, J.C., Millam, J.M., Iyengar, S.S., Tomasi, J., Barone, V., Mennucci, B., Cossi, M., Scalmani, G., Rega, N., Petersson, G.A., Nakatsuji, H., Hada, M., Ehara, M., Toyota, K., Fukuda, R., Hasegawa, J., Ishida, M., Nakajima, T., Honda, Y., Kitao, O., Nakai, H., Klene, M., Li, X., Knox, J.E., Hratchian, H.P., Cross, J.B., Adamo, C., Jaramillo, J., Gomperts, R., Stratmann, R.E., Yazyev, O., Austin, A.J., Cammi, R., Pomelli, C., Ochterski, J.W., Ayala, P.Y., Morokuma, K., Voth, G.A., Salvador, P., Dannenberg, J.J., Zakrzewski, V.G., Dapprich, S., Daniels, A.D., Strain, M.C., Farkas, O., Malick, D.K., Rabuck, A.D., Raghavachari, K., Foresman, J.B., Ortiz, J.V., Cui, Q., Baboul, A.G., Clifford, S., Cioslowski, J., Stefanov, B.B., Liu, G., Liashenko, A., Piskorz, P., Komaromi, I., Martin, R.L., Fox, D.J., Keith, T., Al-Laham, M.A., Peng, C.Y., Nanayakkara, A., Challacombe, M., Gill, P.M.W., Johnson, B., Chen, W., Wong, M.W., Gonzalez, C., and Pople, J.A., *Gaussian 03* (2004).
- 35 Turner, E.A., Pye, C.C., and Singer, R.D., Use of *ab initio* calculations toward the rational design of room temperature ionic liquids, *J. Phys. Chem. A* **107**, 2277–2288 (2003).
- 36 Tsuzuki, S., Arai, A.A., and Nishikawa, K., Conformational analysis of 1-butyl-3-methylimidazolium by CCSD(T) level *ab initio* calculations: Effects of neighboring anions, *J. Phys. Chem. B* **112**, 7739–7747 (2008).

- 37 Imanari, M., Uchida, K., Miyano, K., Seki, H., and Nishikawa, K., NMR study on relationships between reorientational dynamics and phase behaviour of room-temperature ionic liquids: 1-alkyl-3-methylimidazolium cations, *Phys. Chem. Chem. Phys.* **12**, 2959–2967 (2010).
- 38 Kojima, A., Yoshimura, Y., Iwasaki, H., and Tozaki, K., Millikelvin-stabilized cell for the precise study of phase transitions, in D.C. Ripple (ed.), *Temperature: Its Measurement and Control in Science and Industry*, Vol. 7, AIP Conference Proceedings, American Institute of Physics, **684**, 921–926 (2003).
- 39 Morrow, T.I., and Maginn, E.J., Molecular dynamics study of the ionic liquid 1-*n*-butyl-3-methylimidazolium hexafluorophosphate, *J. Phys. Chem. B* **106**, 12807–12813 (2002).
- 40 Antony, J.H., Mertens, D., Breitenstein, T., Dölle, A., Wasserscheid, P., and Carper, W.R., Molecular structure, reorientational dynamics, and intermolecular interactions in the neat ionic liquid 1-butyl-3-methylimidazolium hexafluorophosphate, *Pure Appl. Chem.* **76**, 255–261 (2004).
- 41 Urahata, S.M., and Ribeiro, M.C.C., Single particle dynamics in ionic liquids of 1-alkyl-3-methylimidazolium cations, *J. Chem. Phys.* **122**, 024511–024519 (2005).
- 42 Choudhury, A.R., Winterton, N., Steiner, A., Cooper, A.I., and Johnson, K.A., In situ crystallization of low-melting ionic liquids, *J. Am. Chem. Soc.* **127**, 16792–16793 (2005).
- 43 Dibrov, S.M., and Kochi, J.K., Crystallographic view of fluidic structures for room-temperature ionic liquids: 1-Butyl-3-methylimidazolium hexafluorophosphate, *Acta Crystallogr.* **C62**, o19–o21 (2006).
- 44 Kabo, G.J., Blokhin, A.V., Paulechka, Y.U., Kabo, A.G., Shymanovich, M.P., and Magee, J.W., Thermodynamic properties of 1-butyl-3-methylimidazolium hexafluoro-phosphate in the condensed state, *J. Chem. Eng. Data* **49**, 453–461 (2004).
- 45 Jin, H., O'Hare, B., Dong, J., Arzhantsev, S., Baker, G.A., Wishart, J.F., Benesi, A.J., and Maroncelli, M., Physical properties of ionic liquids consisting of the 1-butyl-3-methylimidazolium cation with various anions and the bis(trifluoromethylsulfonyl) imide anion with various cations, *J. Phys. Chem. B* **112**, 81–92 (2008).
- 46 Triolo, A., Mandanici, A., Russina, O., Rodriguez-Mora, V., Cutroni, M., Hardacre, C., Nieuwenhuyzen, M., Bleif, H.-J., Keller, L., and Ramos, M.A., Thermodynamics, structure, and dynamics in room temperature ionic liquids: The case of 1-butyl-3-methyl imidazolium hexafluorophosphate ([bmim][PF₆]), *J. Phys. Chem. B* **110**, 21357–21364 (2006).
- 47 Domańska, U., and Marciniak, A., Solubility of 1-alkyl-3-methylimidazolium hexafluoro-phosphate in hydrocarbons, *J. Chem. Eng. Data* **48**, 451–456 (2003).
- 48 Troncoso, J., Cerdeiriña, C.A., Sanmamed, Y.A., Romaní, L., and Rebelo, L.P.N., Thermodynamic properties of imidazolium-based ionic liquids: Densities, heat capacities, and enthalpies of fusion of [bmim][PF₆] and [bmim][NTf₂], *J. Chem. Eng. Data* **51**, 1856–1859 (2006).
- 49 Paulechka, Y.U., Kabo, G.J., Blokhin, A.V., Shaplov, A.S., Lozinskaya, E.I., Golovanov, D.G., Lyssenko, K.A., Korlyukov, A.A., and Vygodskii, Y.S., IR and X-ray study of polymorphism in 1-alkyl-3-methylimidazolium bis(trifluoromethane sulfonyl)imides, *J. Phys. Chem. B* **113**, 9538–9546 (2009).

- 50 Nakakoshi, M., Shiro, M., Fujimoto, T., Machinami, T., Seki, H., Tashiro, M., and Nishikawa, K., Crystal structure of 1-butyl-3-methylimidazolium iodide, *Chem. Lett.* **35**, 1400–1401 (2006).
- 51 Santos, C.S., Rivera-Rubero, S., Dibrov, S., and Baldelli, S., Ions at the surface of a room-temperature ionic liquid, *J. Phys. Chem. C* **111**, 7682–7691 (2007).
- 52 Yoshida, R., Takahashi, T., Yamaguchi, T., and Ichijo, H., Self-oscillating gel, *J. Am. Chem. Soc.* **118**, 5134–5135 (1996).